



Upconversion luminescence mediated photodynamic therapy through hydrophilically engineered porphyrin

Xiaodan Sun^{a,b,1}, Peisen Zhang^{a,b,1}, Yi Hou^{a,*}, Yingying Li^{a,b}, Xiaodan Huang^{a,b}, Zihua Wang^a, Lihong Jing^{a,*}, Mingyuan Gao^{a,b,*}

^a Key Laboratory of Colloid, Interface and Chemical Thermodynamics, Institute of Chemistry, Chinese Academy of Sciences, Bei Yi Jie 2, Zhong Guan Cun, Beijing 100190, China

^b School of Chemistry and Chemical Engineering, University of Chinese Academy of Sciences, Beijing 100049, China

ARTICLE INFO

Keywords:

Upconversion nanoparticles
Porphyrin
Click reaction
Photodynamic therapy
Efficacy

ABSTRACT

Photodynamic therapy that involves the photosensitizer transferring the absorbed energy to surrounding tissue oxygen has been used in clinical treatment of cancer. However, the clinically used porphyrin derivatives as PDT photosensitizers usually need high energy excitation light, which generally gives rise to limited tissue penetration depth and thereby limited photoactivation efficiency. Herein, protoporphyrin IX was chemically modified by jeffamines for improving the hydrophilicity and biocompatibility, and the resulting water-soluble porphyrin-jeffamine (PJ) was further covalently conjugated to the PEGylated upconversion nanoparticles (UCNPs) via “click” reaction, which is an efficient way to precisely control the resonance energy transfer from UCNPs to PJs. Our work demonstrates that, the probes can be effectively photosensitized to produce reactive oxygen species (ROS) under the excitation of 980 nm NIR light. When compared with the clinically used photosensitizer molecules, the probes exhibit a comparable capability for producing ROS. Besides, the probes present an outstanding ability in targeting tumor cells and high efficiency in inducing cell death through the photoactivation by 980 nm laser.

1. Introduction

Photodynamic therapy (PDT), as a non-invasive and selective medical technology, has been applied for clinical treatment of pre- and malignant tumors [1–5]. PDT is based on the administration of photosensitizers (PSs), which can be activated by light to generate reactive oxygen species (ROS), leading to cell death [6–10]. Up to now, the majority of clinically used PSs are porphyrin derivatives [11–13], such as hematoporphyrin monomethyl ether (HMME) [14,15]. The optimal excitation windows for these PSs are in the visible or even UV range [16], which exhibit limited tissue penetration depth due to the strong tissue absorption and scattering of lights, and thus reduce the therapeutic effects of PDT on internal tumors. Therefore, it is one of the main challenges for PDT to properly balance the photoactivation efficiency and penetration depth of excitation light.

The rare earth based upconversion nanoparticles (UCNPs) serving as ultra-sensitive optical nanoprobe for *in vivo* imaging provide a new perspective to circumvent this limitation [17–24]. Upconversion

luminescence (UCL) is an anti-Stokes process, which can convert the near-infrared (NIR) light to shorter wavelength light [25–30]. As biological tissues exhibit significantly decreased light absorption and scattering for NIR light in the wavelength range of 700–1300 nm in comparison with those for visible light, NIR light is preferable for reaching deeper tissues [31–36]. It has been demonstrated that, UCNPs can serve as nanocarriers and light transducers to activate PSs in deep tissues [37]. For instance, UCNPs attached with Chlorin e6 (a porphyrin derivative) through hydrophobic interaction between the PSs molecules and surface ligands of UCNPs, have been reported to achieve upconversion-mediated PDT of tumors *in vivo* [38]. The UCL can realize the activation of PSs located deeply in lesions, which is apparently helpful for reducing the dose of PSs to alleviate possible side effects, while the upconversion nanoparticles promote the accumulation of PSs in tumor tissues due to the enhanced permeability and retention (EPR) effect. However, the structures of the literature-reported UCNP-PSs composites were mainly fabricated through physical adsorption such as hydrophobic interactions [39–41], because the majority of PS molecules

* Corresponding authors at: Key Laboratory of Colloid, Interface and Chemical Thermodynamics, Institute of Chemistry, Chinese Academy of Sciences, Bei Yi Jie 2, Zhong Guan Cun, Beijing 100190, China.

E-mail addresses: gaomy@iccas.ac.cn (M. Gao), jinglh@iccas.ac.cn (L. Jing), houyi@iccas.ac.cn (Y. Hou).

¹ These authors contributed equally to this work.

<https://doi.org/10.1016/j.cep.2019.107551>

Received 7 April 2019; Received in revised form 15 May 2019; Accepted 30 May 2019

Available online 05 June 2019

0255-2701/ © 2019 Elsevier B.V. All rights reserved.

exhibit poor water-solubility. In consequence, the PSs attached on the particle surface *via* physical interaction may suffer from non-specific release during circulation in blood stream before they reach the tumorous site, due to the complex interactions between the photosensitizer molecules and biomolecules in different tissues, which may give rise to unfavorable biodistribution of the PSs and bring phototoxicity to tissues of the body surface. In this context, to increase the stability of the probe by covalently attaching the PSs on the surface of the UCNPs will be helpful for better controlling the biodistribution of the PSs carried by the nanoparticles. On the other hand, in the composite probe formed through hydrophobic-hydrophobic interaction between PSs and surface ligands of a nanocarrier, it is very difficult to control the relative distance between PSs and underlying carrier, which is however very important for effectively transferring the UCNP photon energy into ROS through the PSs. Although different conjugation strategies are being developed [39], there still lacks a reliable approach for achieving stable UCNP-PSs conjugates with controllable loading capacity of PSs.

Following our previous studies on UCL nanoprobe for tumor imaging [17,18,42,43], herein we propose a novel approach for constructing UCNP-based PDT sensitizers. As depicted in Fig. 1, protoporphyrin IX was chosen as model PDT sensitizer and it was covalently conjugated with jeffamine molecules *via* amidation reaction in order to improve the hydrophilicity. Upon further “click” reaction [44,45] between the thiolated PS and the maleimide group on the UCNP surface, the stable probes with different loading amounts of PSs on UCNPs were obtained. The PDT treatment of cancer cells under NIR light was further performed based on the UCNP-PSs probe.

2. Materials and methods

2.1. Chemicals

The following materials were purchased from Sigma-Aldrich: $\text{GdCl}_3 \cdot 6\text{H}_2\text{O}$ (G7532), $\text{YbCl}_3 \cdot 6\text{H}_2\text{O}$ (337927), $\text{ErCl}_3 \cdot 6\text{H}_2\text{O}$ (289256), oleic acid (OA, 364525), 1-octadecene (ODE, O806), ammonium fluoride (NH_4F , 216011), thiazolyl blue tetrazolium bromide (MTT, M2128), *N,N*-dimethyl-4-nitrosoaniline (RNO, D172405), 2-

iminethiolane hydrochloride (2IT, I6256), 2,2'-(ethylenedioxy)bis(ethylamine) (Jeffamine, 385506), 4-(4,6-Dimethoxy-1,3,5-triazin-2-yl)-4-methylmorpholinium chloride (DMTMM, 74104), protoporphyrin IX (P103197), imidazole (I108707) were purchased from Aladdin. Analytical grade chemicals such as methanol, ethanol, cyclohexane, ether, and tetrahydrofuran (THF) were purchased from Sinopharm Chemical Reagent Beijing, Co., Ltd. A bifunctional ligand, PEG2000, bearing a maleimide group at one end and a diphosphate group at the other end (mal-PEG-dp) was a custom-made product provided by Beijing Oneder Hightech Co., Ltd. Human colorectal cancer cell line LS180 were obtained from the oncology school of Peking University. Hematoporphyrin monomethyl ether (HMMME, S61821) was purchased from Shanghai Yuanye Biotechnology Co., Ltd. DMEM/F12 (1:1) (1x), 0.25% trypsin-EDTA (1x) were purchased from Gibco. Phosphate buffer saline, penicillin-streptomycin solution were purchased from Beijing Solarbio Science & Technology Co., Ltd. Fetal bovine serum (FBS) was purchased from Zhejiang Tianhang Biotechnology Co., Ltd. Dimethyl sulfoxide was purchased from Amersco. Other solvents and chemicals were used without further purification.

2.2. Synthesis of $\text{NaGdF}_4:\text{Yb,Er}$ UCNPs

The $\text{NaGdF}_4:\text{Yb,Er}$ UCNPs were synthesized following our previous protocol with some modifications [17]. In a typical synthesis, $\text{GdCl}_3 \cdot 6\text{H}_2\text{O}$ (0.480 mmol), $\text{YbCl}_3 \cdot 6\text{H}_2\text{O}$ (0.108 mmol), and $\text{ErCl}_3 \cdot 6\text{H}_2\text{O}$ (0.012 mmol) were mixed with 4 mL OA and 16 mL ODE in a 100 mL three-neck round-bottom flask. The resultant mixture was heated to 150 °C under vacuum condition. After a homogeneous solution was formed, the solution was cooled down to 50 °C, and a methanol solution of 10 mL containing NaOH (1.8 mmol) and NH_4F (1.8 mmol) was introduced dropwise. The reaction system was then kept under stirring at this temperature for 30 min. After that, the reaction temperature was increased to 100 °C under vacuum condition to remove the methanol from the reaction mixture. Upon removal of methanol, the solution was quickly heated to 300 °C under nitrogen protection and reacted for 1 h. The resultant nanoparticles were precipitated by ethanol, collected by centrifugation, washed with ethanol for three times, and finally redispersed in cyclohexane for further experiments.

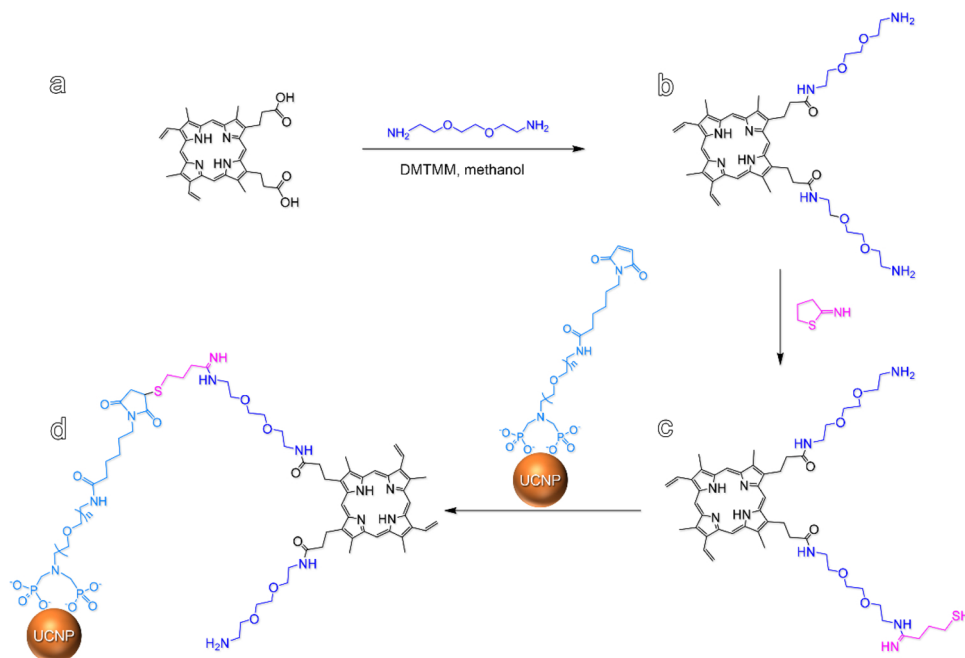


Fig. 1. Synthesis routes of the probe based on upconversion nanoparticles (UCNPs). Protoporphyrin IX (a), porphyrin-jeffamine (PJ) (b), thiolated porphyrin-jeffamine (c), and UCNP-PJ probe (d).

2.3. Synthesis of core-shell NaGdF₄:Yb,Er@NaGdF₄ UCNPs

Subsequent deposition of NaGdF₄ shell followed a similar process for the preparation of NaGdF₄:Yb,Er core particles. Briefly, 0.5 mmol GdCl₃·6H₂O was added to a 100 mL three-neck round-bottom flask containing 4 mL OA and 16 mL ODE. The resultant mixture was heated to 150 °C under vacuum condition. After a homogeneous solution was formed, the solution was cooled down to 80 °C, and then 0.5 mmol NaGdF₄:Yb,Er nanoparticles dispersed in 5 mL cyclohexane were introduced into the above solution. After heated to 150 °C to remove the cyclohexane, the solution was cooled down to 50 °C. Subsequently, a methanol solution of 5 mL containing NaOH (0.9 mmol) and NH₄F (0.9 mmol) was added dropwise. The reaction system was then kept under stirring at this temperature for 30 min. After that, the reaction temperature was increased to 100 °C under vacuum condition to remove the methanol from the reaction mixture. Upon removal of methanol, the solution was quickly heated to 300 °C under nitrogen protection and reacted for 1 h. The obtained core-shell nanoparticles were precipitated by ethanol, collected by centrifugation, washed with ethanol for three times, and finally redispersed in THF for further experiments.

2.4. Synthesis of PEGylated NaGdF₄:Yb,Er@NaGdF₄ UCNPs

The PEGylated UCNPs were prepared through a ligand exchange approach according to our previous report [17]. Approximately 10 mg of purified core-shell UCNPs and 100 mg of mal-PEG-dp were dissolved in 5 mL THF, and the mixture was kept stirring overnight at 40 °C. Then the PEGylated UCNPs were precipitated and washed with cyclohexane for three times, and finally dried under vacuum condition at room temperature. The obtained solid substance was then dissolved in Milli-Q water and removed the free ligand by ultrafiltration (Millipore YM-100) for further experiments.

2.5. Synthesis of porphyrin-jeffamine conjugate

Firstly, 50 mg of protoporphyrin IX and 60 mg of DMTMM were dissolved in 4 mL methanol. Then, 400 µL jeffamine was dropwise added into the above solution. The reaction solution was kept stirring at room temperature in the dark environment overnight. The resultant mixture was firstly centrifuged to remove the insoluble, and then the supernatant solution was precipitated and washed with anhydrous ether for three times. After being dried under vacuum condition, the resulting porphyrin-jeffamines (PJs) can be readily dissolved in Milli-Q water for further experiments.

2.6. Synthesis of UCNP-PJ probe

Typically, the obtained PJs were subjected to thiolation by 2IT at the mole ratio of 1:1.2 to convert part of the amino groups to thiol ones. After mixed with the PEGylated UCNPs, the covalently conjugates (UCNP-PJs) were obtained via “click” reaction. Free PJs were removed by ultrafiltration (Millipore YM-30). The formed conjugates were suspended in water and stored at 4 °C for further use. UV-vis absorption spectra were measured by using a Cary 50 UV-vis spectrophotometer. The loading amounts of PJs onto PEGylated UCNPs were determined by the absorbance peak at 640 nm (characteristic of PJ, after subtracting the absorbance of PEGylated UCNPs at this wavelength) according to a standard curve of PJ.

2.7. Determination of ROS

ROS were determined following previous procedures [46,47]. Typically, the probes were mixed with RNO (50 µM) and imidazole (50 µM) in 20 mM phosphate buffer (pH = 7.4). The resultant solutions were then irradiated by a 980 nm or 635 nm laser (0.5 W/cm²) for

different periods of time. The generation of singlet oxygen by probes would result in bleaching of RNO absorption at 440 nm. The ratio of the reduced optical density to the initial value at 440 nm thus reflects the production of ROS.

2.8. Cellular staining

According to our previous work [48], approximately 1×10^4 LS180 cancer cells per well were seeded on a 96-well cell culture plate and incubated overnight at 37 °C under 5% CO₂ to allow a firm adherence. Then 100 µL of solutions containing probes (100 µg/mL) or UCNPs (100 µg/mL) were added into each well and incubated with the cells for 4 h, respectively. After the supernatant was decanted, the cells were rinsed three times with $1 \times$ PBS buffer to remove the unbound particles and fixed in 4% paraformaldehyde. Then the cells were incubated with the staining solution containing chlorophosphonazo III (20 µg/mL) and HNO₃ (0.03 M) for 20 min, washed with Milli-Q water, and then subjected to microscopy study.

2.9. In vitro PDT evaluation of probes

MTT assays were carried out on LS180 cell lines. Cells were seeded into a 96-well cell culture plate by 5×10^3 cells/well under 100% humidity, and then cultured at 37 °C in an atmosphere containing 5% CO₂ for 24 h. The probes were added to the wells at a series of gradient concentrations for 4 h and exposed to an irradiation (980 nm) with a power density of 1.0 W/cm² for 10 min (1 min interval after each minute of irradiation) after the probes were decanted, while the cells treated with the same procedures without irradiation were set as controls. Then cells in both experimental and control groups were incubated for another 24 h at 37 °C under 5% CO₂. After that, 10 µL of MTT (5 mg/mL) was added to each well and incubated for 4 h at 37 °C under 5% CO₂. Then, 150 µL of DMSO was added into per well, and the assay plate was shaken at 37 °C for 15 min. The optical density of each well at 490 nm was recorded on a microplate reader (Thermo, Varioskan Flash), while the optical density at 630 nm was used as reference.

2.10. Characterization

Transmission Electron Microscopy (TEM) measurements were carried out with a JEM-100CXII microscope operating at an accelerating voltage of 100 kV for characterizing the core and core-shell UCNPs. Powder X-ray diffraction (XRD) patterns were obtained with a Regaku D/Max-2500 diffractometer equipped with a Cu Kα₁ radiation ($\lambda = 1.54056 \text{ \AA}$). The UCL spectra were recorded on a Cary Eclipse fluorescence spectrophotometer equipped with a 980 nm CW laser diode (0–2 W) serving as the excitation source. The concentration of rare earth elements in the nanoparticles was determined by using inductively coupled plasma atomic emission spectrometer (ICP-AES, Thermo ICP 6300). ¹H NMR spectra were recorded at 400 MHz (Bruker). The chemical shifts were reported in parts per million (ppm) using acetic acid-D₄ as the solvent. Dynamic light scattering (DLS) was carried out at 298.0 K with a Zetasizer Nano ZS (Malvern) equipped with a solid-state He-Ne laser ($\lambda = 633 \text{ nm}$) for monitoring the variation of hydrodynamic sizes of the nanoparticles before and after PJs conjugation.

3. Results and discussion

3.1. Structural analysis of UCNPs

The TEM images and their corresponding size distributions for NaGdF₄:Yb,Er core and core-shell NaGdF₄:Yb,Er@NaGdF₄ UCNPs are shown in Fig. 2a–b. Both of them show spherical morphology and high degree of monodispersity with respective average size of

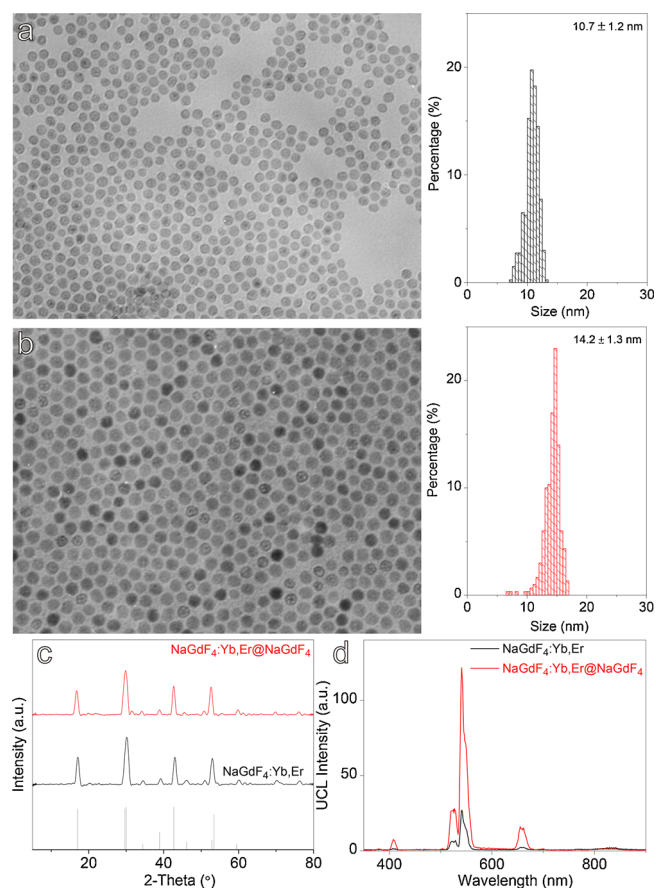


Fig. 2. TEM images and size distributions of NaGdF₄:Yb,Er core nanoparticles (a), and NaGdF₄:Yb,Er@NaGdF₄ core-shell nanoparticles (b), together with their XRD patterns (the vertical line pattern in the bottom frame is the standard XRD data for hexagonal NaGdF₄ according to JCPDS card (No. 27-0699)) (c), and the upconversion luminescence (UCL) spectra of nanoparticles recorded under 980 nm laser excitation (d).

10.7 ± 1.2 nm and 14.2 ± 1.3 nm. The particle size distribution, defined by the relative standard deviation (RSD) of the particle size, decreased from 11% for cores to 9% for core-shell ones, suggesting that no second nucleation occurred during the shell coating process. Powder X-ray diffraction patterns exhibited in Fig. 2c demonstrate that the core and core-shell particles are in consistent with hexagonal NaGdF₄ phase.

3.2. Optical properties of UCNPs

The UCL spectra of as-prepared NaGdF₄:Yb,Er nanoparticles and core-shell NaGdF₄:Yb,Er@NaGdF₄ nanoparticles dispersed in cyclohexane are shown in Fig. 2d. The emission peaks locating at 410 nm, 520 nm, 540 nm, and 655 nm are attributed to radiative relaxations from ²H_{9/2}, ²H_{11/2}, ⁴S_{3/2}, and ⁴F_{9/2} excited states to the ⁴I_{15/2} ground state of Er³⁺, respectively. The upconversion luminescence was significantly enhanced by a factor of 4 after epitaxial shell growth. The improvement can be attributed to that, the shell coating efficiently reduced the non-radiative transition channels associated with the surface defects and organic ligands [49].

3.3. Properties of UCNP-PJ probes

The hydrophilic PJ was synthesized through the amidation between carboxyl groups in protoporphyrin IX and amino groups in jeffamine as shown in Fig. 1. The chemical structures of protoporphyrin IX before and after conjugation with jeffamine were characterized by ¹H nuclear magnetic resonance (¹H NMR) spectroscopy as shown in Fig. 3. The

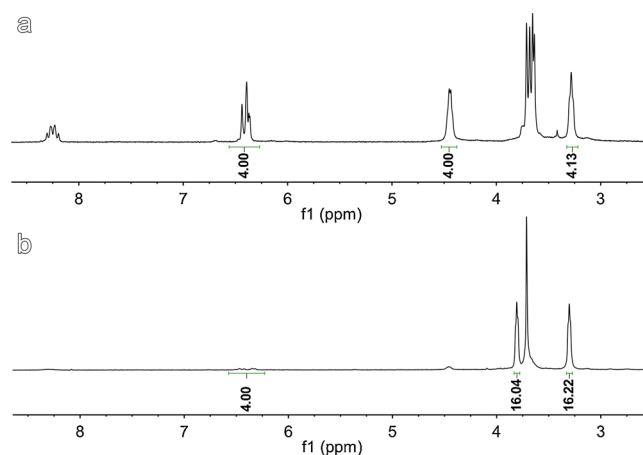


Fig. 3. ¹H NMR spectra of protoporphyrin IX (a), and PJ (b).

ratio of -CH₂- to -CH=CH₂ increased from 2:1 to 8:1 after conjugation, suggesting each protoporphyrin IX was successfully conjugated with two jeffamine molecules. The loading of the obtained hydrophilic PJs on the PEGylated UCNPs was realized through the “click” reaction between the thiol group in the thiolated PJ and maleimide group on the surface of UCNP as shown in Fig. 1. After free PJs were removed by ultrafiltration, the UV-vis spectra of resulting UCNP-PJ probes with different loading amounts of PJs were measured as shown in Fig. 4a. The loading amounts of PJs on the surface of UCNPs were determined by the absorbance at 640 nm (characteristic of PJ, after subtracting the absorbance of PEGylated UCNPs at the same wavelength) according to a standard curve of PJ (Fig. S1). It was found that the amounts of covalently conjugated PJs calculated according to the standard curve were consistent with theoretical ones, which suggests that the efficiency of the “click” reaction between thiol group and maleimide group is near 100%. Therefore, the loading amounts of PJs on the UCNPs surface can be precisely controlled simply through adjusting feeding amounts of PJs. The average number of PJ molecules per UCNP was determined to be about 118 for UCNP-PJ conjugates (2.0% w/w, PJ:UCNP). The above results demonstrate that the highly efficient “click” reaction is helpful to control the distance between the PJs and the underlying UCL nanocarrier in effectively transferring the photon energy of UCNP into ROS through the PJs.

The colloidal stability of UCNPs and UCNP-PJ probes were characterized by DLS analysis as is shown in Fig. 4b. The hydrodynamic size (HD) of core-shell UCNPs exhibits a narrow single scattering peak at 37.8 nm, after conjugated with PJs, the HD of the resulting probes increased to 38.0 nm, 43.8 nm, and 50.7 nm, according to the feeding amounts of 0.5%, 1.0%, and 2.0% (w/w, PJ:UCNP), respectively. The zeta potential of resulting UCNP-PJ probes (2.0%) was determined to be about 12.3 mV. The reasonable increment in hydrodynamic size and no additional light scattering peaks appeared after conjugation with PJ molecules, indicate that the reaction occurred in a controlled manner.

According to the UCL emission spectra of the probes with different PJ loading concentrations with a 980 nm laser as the excitation source, it is clear that the conjugation of PJs on nanoparticles induces a significant quenching of luminescence (Fig. 4c), which demonstrates that effective luminescence resonance energy transfer (LRET) occurred from the UCNPs to loaded PJs possessing strong absorption in the range of 400–600 nm.

3.4. Generation of ROS

Generation of cytotoxic ROS from UCNP-PJs is critical for PDT. It was evaluated through monitoring the absorption of RNO in the presence of imidazole. The capture of ROS by imidazole ring gives rise to a trans-annular peroxide intermediate, which then reacts with RNO and

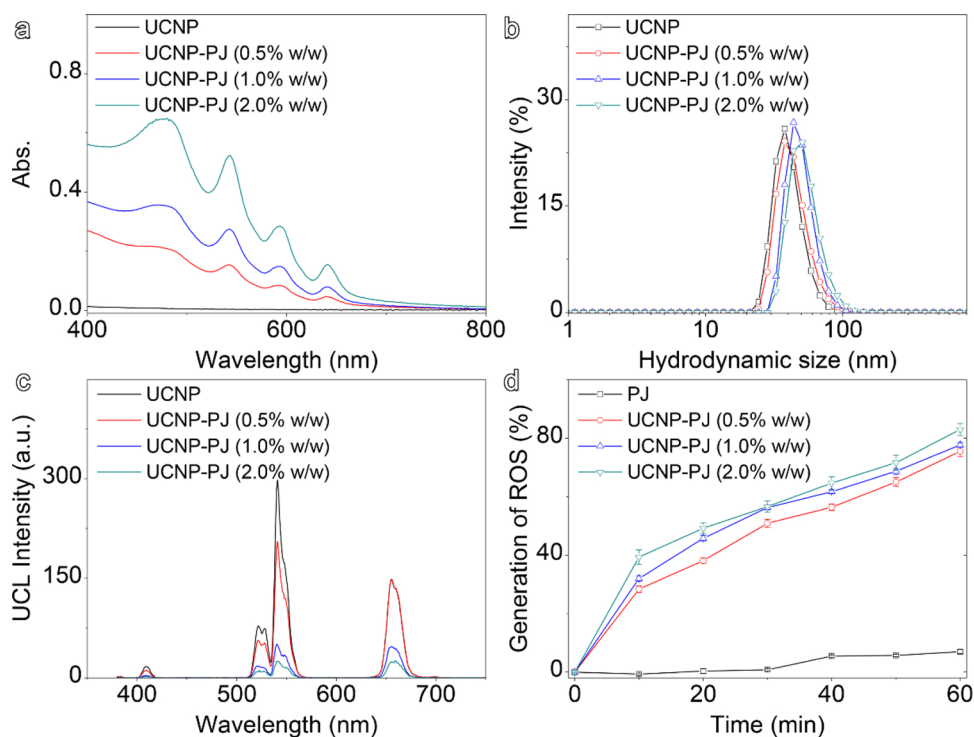


Fig. 4. UV-vis absorption spectra (a), hydrodynamic size distribution profiles (b), UCL spectra under 980 nm laser excitation (c), and time dependent ROS generation under 980 nm laser excitation (d) of different loading concentrations of PJ on the PEGylated UCNPs. The generation of ROS is determined by the relative bleaching of RNO absorbance at 440 nm.

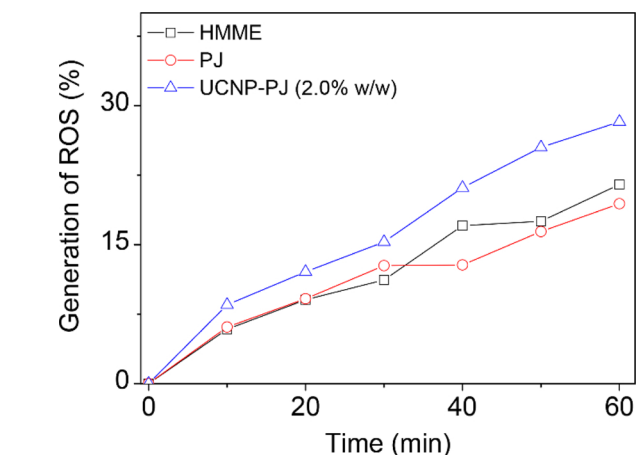


Fig. 5. Time-dependent ROS generation by HMME, PJ, and UCNP-PJ probes under 635 nm excitation. The generation of ROS was determined by the relative bleaching of RNO absorbance at 440 nm.

induces the bleaching of RNO. The amounts of ROS produced by PSs could then be determined by the ratio of the reduced absorbance of RNO at 440 nm to the initial value.

As is shown in Fig. 4d, when the UCNP-PJ probes (containing 2.5 mg/mL UCNPs) bearing different loading amounts of PJs were exposed to the 980 nm laser at a power density of 0.5 W/cm^2 , the ROS produced from the probes significantly increased against the irradiation time. In contrast, UCNPs without conjugation of PJs was not able to generate ROS under 980 nm irradiation. Furthermore, the amounts of ROS generated by UCNP-PJ probes are positively correlated with the loading concentrations of PJ with the same irradiation time. Therefore, UCNP-PJ probes are able to efficiently generate ROS through transferring the UCL of nanoparticles to surface conjugated PJ molecules. As a representative, the UCNP-PJ (2.0%, w/w) probe with highest amounts of ROS generation was chosen for further experiments.

The ROS generated through UCNP-PJ ($5 \mu\text{M}$ of PJs) probes were further compared with both clinically used HMME ($5 \mu\text{M}$) and synthesized PJs only ($5 \mu\text{M}$) under the irradiation of 635 nm laser at a power density of 0.5 W/cm^2 , as shown in Fig. 5, (corresponding absorption spectra shown in Fig. S2). The UCNP-PJ probes are capable of

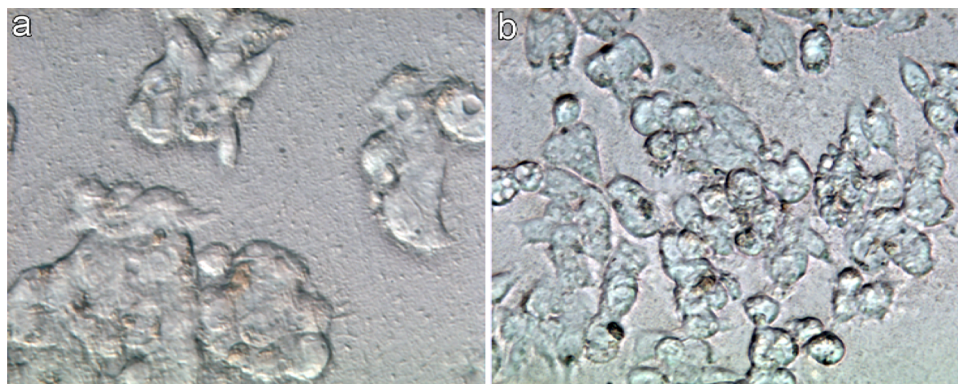


Fig. 6. The cellular staining with chlorophosphonazo III incubated with UCNPs (a) and UCNP-PJ probes (b) for 4 h.

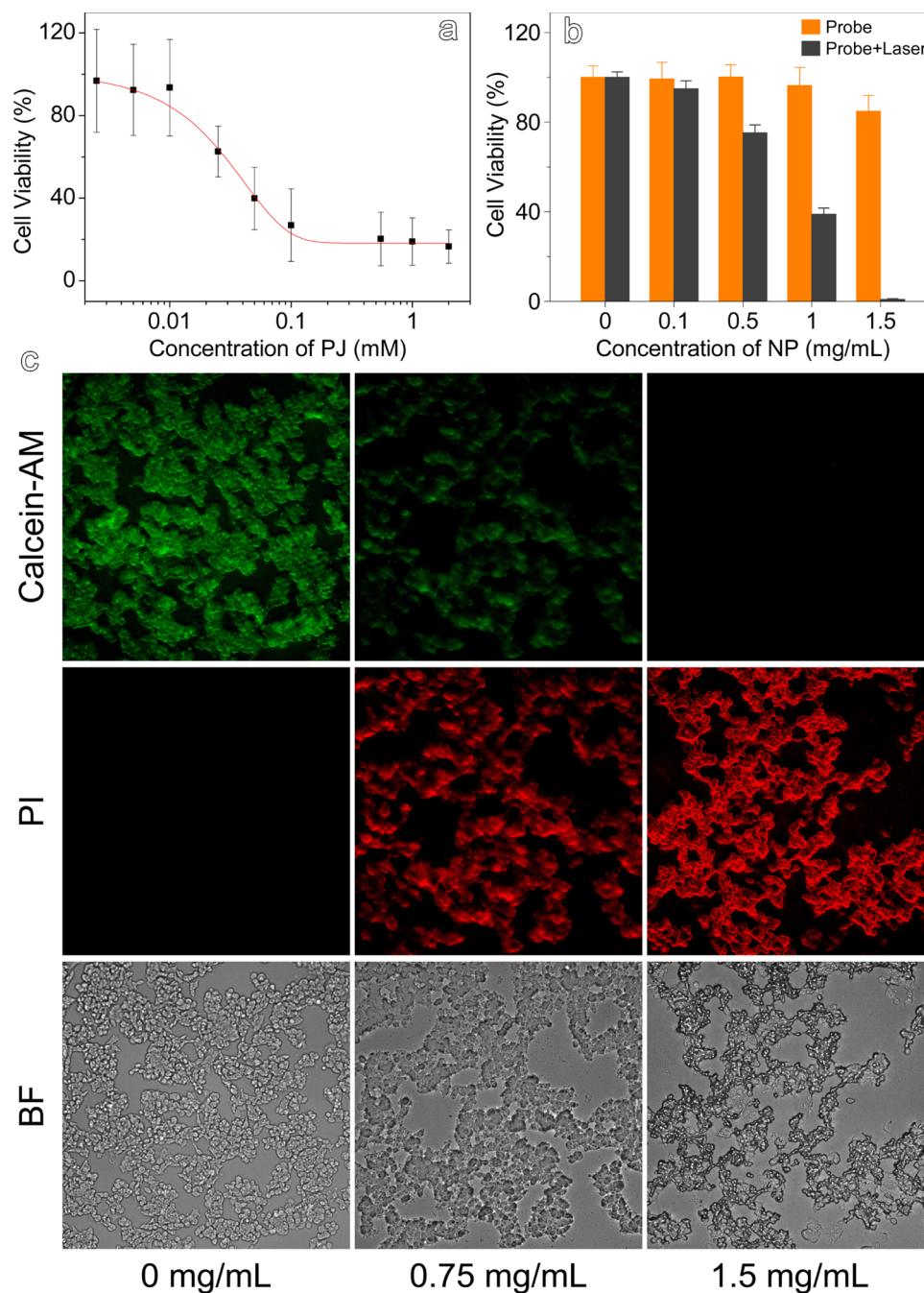


Fig. 7. *In vitro* cell experiments. (a) Relative cell viabilities of LS180 after being incubated with various concentrations of PJ for 24 h. (b) Relative cell viabilities of LS180 after being incubated with various concentrations of probe (2.0%, w/w) under 980 nm laser excitation (1 W/cm², 10 min). (c) Live-dead cell staining kit stained images of LS180 incubated with probe (2.0%, w/w) at different concentrations after 980 nm laser excitation (1 W/cm², 10 min).

producing highest amounts of ROS compared to either HMME or PJs during irradiation, which may be induced by a synergistic effect between the UCNPs and PJs. Furthermore, it was found out that the UCNP-PJ probes irradiated under 980 nm laser exhibit comparable efficiency in generation of cytotoxic ROS in comparison with that of the clinically used HMME excited at 635 nm with the same irradiation density.

3.5. *In vitro* PDT treatment of cancer cells

The UCNP-PJ probes are expected to possess tumor targeting ability, as porphyrins can be captured by low density lipoprotein (LDL) receptors on the surfaces of cancer cells and enter the cells through

receptor-mediated endocytosis [50]. Therefore, the specific binding assay was performed using LS180 cells which highly express LDL receptors on their surfaces. Specifically, the cells were incubated with UCNP-PJ probes for 4 h, and then subjected to microscopy observation after staining with chlorophosphonazo III in acidic range. As shown in Fig. 6, the cells treated with probes clearly turned cyan, yet no obvious color changing can be seen in the cells incubated with UCNPs only, which indicates that the cell uptake of the probes is much higher than that of UCNPs, *i.e.*, the UCNP-PJ probes have obvious targeting ability towards cancer cells.

As is shown in Fig. 7a, the IC₅₀ of free PJs without irradiation is 40 μM, which indicates good biocompatibility of PJs and UCNP-PJ probes (Fig. S3). Considering the excellent photodynamic performance

of the probes, *in vitro* PDT treatment of cancer cells was evaluated through MTT assay. LS180 cells were incubated with probes at a series of concentrations for 4 h and then exposed to an irradiation (980 nm) with a power density of 1.0 W/cm² for 10 min (1 min interval after each minute of irradiation, which has been indicated that simple laser irradiation had no effect on cells (Fig. S4)), while the cells treated with probes only in absence of laser were used as the control. As is shown in Fig. 7b, the cell viability decreased drastically with the increased probe concentrations after irradiation, which is close to zero at 1.5 mg/mL UCNPs (containing 36 μM of PJs, which is under the safe dose of PJs). As for the control group, the cell viability remained above 95% after incubation with 1.0 mg/mL UCNPs (containing 24 μM PJs), and 85% of the cells still survived at 1.5 mg/mL UCNPs (containing 36 μM PJs). It is concluded that within the safe doses of PJs and probes, our probes show high efficiency of photoactivation in producing cytotoxic ROS to kill the cancer cells.

The cancer-killing effects of probes were further demonstrated by staining the cells with a Live-Dead Cell Staining Kit after laser irradiation to differentiate the live and dead cells. Most cells were destroyed after incubation with 1.5 mg/mL of UCNPs-PJ probes exposed to irradiation with a 980 nm laser (Fig. 7c). In contrast, only very limited cancer cells died if not incubated with probes after exposed to laser irradiation. These results demonstrate that the UCNPs-PJ probes could serve as a potential UCL-mediated PDT agent for ablation of cancer cells.

4. Conclusions

We have successfully synthesized hydrophilic and biocompatible PJ molecules. Upon covalently conjugated to the surface of the PEGylated UCNPs through “click” reaction, the obtained UCNPs-PJ probes with stable and controllable structure can be effectively triggered by NIR light through resonance energy transfer from UCNPs to PJs. The probes show comparable capacity for generating ROS when compared with clinically used HMME. *In vitro* experiments indicate that the probes exhibit outstanding targeting ability towards tumor cells and exhibit a high efficiency of photoactivation in generating cytotoxic ROS to induce cell death under the irradiation of 980 nm laser within the safe doses. Compared to the existed PDT nanocarriers realized by the hydrophobic-hydrophobic interaction between PSs and NPs, our work paves a new way in fabricating stable upconversion luminescence mediated PDT nanoagent for the ablation of cancers.

Acknowledgements

This work was supported by the National Key Research Program of China (2018YFA0208800), NSFC (81671754, 81671755, 81720108024, 81530057, 81771902, 81801766), the Youth Innovation Promotion Association CAS (2018042), State Key Laboratory of Luminescence and Applications (SKLA-2019-01).

Appendix A. Supplementary data

Supplementary material related to this article can be found, in the online version, at doi:<https://doi.org/10.1016/j.cep.2019.107551>.

References

- [1] H.I. Pass, Photodynamic therapy in oncology: mechanisms and clinical use, *JNCI-J. Natl. Cancer Inst.* 85 (6) (1993) 443–456, <https://doi.org/10.1093/jnci/85.6.443>.
- [2] T.J. Dougherty, C.J. Gomer, B.W. Henderson, G. Jori, D. Kessel, M. Korbelik, et al., Photodynamic therapy, *JNCI-J. Natl. Cancer Inst.* 90 (12) (1998) 889–905, <https://doi.org/10.1093/jnci/90.12.889>.
- [3] P. Agostinis, K. Berg, K.A. Cengel, T.H. Foster, A.W. Girotti, S.O. Gollnick, et al., Photodynamic therapy of cancer: an update, *CA-Cancer J. Clin.* 61 (4) (2011) 250–281, <https://doi.org/10.3322/caac.20114>.
- [4] A. Punjabi, X. Wu, A. Tokatli-Apollon, M. El-Rifai, H. Lee, Y. Zhang, et al., Amplifying the red-emission of upconverting nanoparticles for biocompatible

- clinically used prodrug-induced photodynamic therapy, *ACS Nano* 8 (10) (2014) 10621–10630, <https://doi.org/10.1021/nn505051d>.
- [5] M.H. Chan, Y.T. Pan, Y.C. Chan, M. Hsiao, C.H. Chen, L.D. Sun, et al., Nanobubble-embedded inorganic 808 nm excited upconversion nanocomposites for tumor multiple imaging and treatment, *Chem. Sci.* 9 (12) (2018) 3141–3151, <https://doi.org/10.1039/C8SC00108A>.
- [6] A.P. Castano, P. Mroz, M.R. Hamblin, Photodynamic therapy and anti-tumour immunity, *Nat. Rev. Cancer* 6 (7) (2006) 535–545, <https://doi.org/10.1038/nrc1894>.
- [7] Á. Juarranz, P. Jaén, F. Sanz-Rodríguez, J. Cuevas, S. González, Photodynamic therapy of cancer. Basic principles and applications, *Clin. Transl. Oncol.* 10 (3) (2008) 148–154, <https://doi.org/10.1007/s12094-008-0172-2>.
- [8] Y. Hou, Z. Zhou, K. Huang, H. Yang, G. Han, Long wavelength light activated prodrug conjugates for biomedical applications, *ChemPhotoChem* 2 (12) (2018) 1005–1011, <https://doi.org/10.1002/cptc.201800147>.
- [9] L. Huang, Z. Li, Y. Zhao, J. Yang, Y. Yang, A.I. Pendharkar, et al., Enhancing photodynamic therapy through resonance energy transfer constructed near-infrared photosensitized nanoparticles, *Adv. Mater.* 29 (28) (2017) 1604789, <https://doi.org/10.1002/adma.201604789>.
- [10] M. Wang, Z. Chen, W. Zheng, H. Zhu, S. Lu, E. Ma, et al., Lanthanide-doped upconversion nanoparticles electrostatically coupled with photosensitizers for near-infrared-triggered photodynamic therapy, *Nanoscale* 6 (14) (2014) 8274–8282, <https://doi.org/10.1039/C4NR01826P>.
- [11] R. Bonnett, Photosensitizers of the porphyrin and phthalocyanine series for photodynamic therapy, *Chem. Soc. Rev.* 24 (1) (1995) 19–33, <https://doi.org/10.1039/C9952400019>.
- [12] M.A. Rajora, J.W.H. Lou, G. Zheng, Advancing porphyrin's biomedical utility via supramolecular chemistry, *Chem. Soc. Rev.* 46 (21) (2017) 6433–6469, <https://doi.org/10.1039/c7cs00525c>.
- [13] R.L. Lipson, E.J. Baldes, A.M. Olsen, The use of a derivative of Hematoporphyrin in tumor detection, *JNCI-J. Natl. Cancer Inst.* 26 (1) (1961) 1–11, <https://doi.org/10.1093/jnci/26.1.1>.
- [14] J. Shi, X. Yu, L. Wang, Y. Liu, J. Gao, J. Zhang, et al., Pegylated Fullerene/Iron oxide nanocomposites for photodynamic therapy, targeted drug delivery and mr imaging, *Biomaterials* 34 (37) (2013) 9666–9677, <https://doi.org/10.1016/j.biomaterials.2013.08.049>.
- [15] X. Ding, Q. Xu, F. Liu, P. Zhou, Y. Gu, J. Zeng, et al., Hematoporphyrin monomethyl ether photodynamic damage on hela cells by means of reactive oxygen species production and cytosolic free calcium concentration elevation, *Cancer Lett.* 216 (1) (2004) 43–54, <https://doi.org/10.1016/j.canlet.2004.07.005>.
- [16] B.S. Wong, S.L. Yoong, A. Jagusiak, T. Pancyk, H.K. Ho, W.H. Ang, et al., Carbon nanotubes for delivery of small molecule drugs, *Adv. Drug Deliv. Rev.* 65 (15) (2013) 1964–2015, <https://doi.org/10.1016/j.addr.2013.08.005>.
- [17] C. Liu, Z. Gao, J. Zeng, Y. Hou, F. Fang, Y. Li, et al., Magnetic/Upconversion fluorescent NaGdF₄:Yb,Er nanoparticle-based dual-modal molecular probes for imaging tiny tumors *in vivo*, *ACS Nano* 7 (8) (2013) 7227–7240, <https://doi.org/10.1021/nn4030898>.
- [18] C. Liu, Y. Hou, M. Gao, Are rare-earth nanoparticles suitable for *in vivo* applications? *Adv. Mater.* 26 (40) (2014) 6922–6932, <https://doi.org/10.1002/adma.201305535>.
- [19] F. Wang, D. Banerjee, Y. Liu, X. Chen, X. Liu, Upconversion nanoparticles in biological labeling, imaging, and therapy, *Analyst* 135 (8) (2010) 1839–1854, <https://doi.org/10.1039/c0an00144a>.
- [20] J. Huang, Y. Hou, C. Liu, L. Jing, T. Ma, X. Sun, et al., Chemical spacer design for engineering the relaxometric properties of core-shell structured rare earth nanoparticles, *Chem. Mat.* 27 (23) (2015) 7918–7925, <https://doi.org/10.1021/acs.chemmater.5b02875>.
- [21] H.S. Mader, P. Kele, S.M. Saleh, O.S. Wolfbeis, Upconverting luminescent nanoparticles for use in bioconjugation and bioimaging, *Curr. Opin. Chem. Biol.* 14 (5) (2010) 582–596, <https://doi.org/10.1016/j.cbpa.2010.08.014>.
- [22] C. Liu, Y. Qi, R. Qiao, Y. Hou, K. Chan, Z. Li, et al., Detection of early primary colorectal cancer with upconversion luminescent NP-based molecular probes, *Nanoscale* 8 (25) (2016) 12579–12587, <https://doi.org/10.1039/c6nr07858j>.
- [23] P. Huang, D. Tu, W. Zheng, S. Zhou, Z. Chen, X. Chen, Inorganic lanthanide nanoprobe for background-free luminescent bioassays, *Sci. China-Mater* 58 (2) (2015) 156–177, <https://doi.org/10.1007/s40843-015-0019-4>.
- [24] X. Sun, J. Sun, B. Dong, G. Huang, L. Zhang, W. Zhou, et al., Noninvasive temperature monitoring for dual-modal tumor therapy based on lanthanide-doped upconversion nanocomposites, *Biomaterials* 201 (2019) 42–52, <https://doi.org/10.1016/j.biomaterials.2019.02.014>.
- [25] L. Zhang, L. Zeng, Y. Pan, S. Luo, W. Ren, A. Gong, et al., Inorganic photosensitizer coupled Gd-based upconversion luminescent nanocomposites for *in vivo* magnetic resonance imaging and near-infrared-responsive photodynamic therapy in cancers, *Biomaterials* 44 (2015) 82–90, <https://doi.org/10.1016/j.biomaterials.2014.12.040>.
- [26] F. Wang, X. Liu, Recent advances in the chemistry of lanthanide-doped upconversion nanocrystals, *Chem. Soc. Rev.* 38 (4) (2009) 976–989, <https://doi.org/10.1039/b809132n>.
- [27] F. Wang, Y. Han, C.S. Lim, Y. Lu, J. Wang, J. Xu, et al., Simultaneous phase and size control of upconversion nanocrystals through lanthanide doping, *Nature* 463 (7284) (2010) 1061–1065, <https://doi.org/10.1038/nature08777>.
- [28] W. Feng, C. Han, F. Li, Upconversion-nanophosphor-based functional nanocomposites, *Adv. Mater.* 25 (37) (2013) 5287–5303, <https://doi.org/10.1002/adma.201301946>.
- [29] L.D. Sun, Y.F. Wang, C.H. Yan, Paradigms and challenges for bioapplication of rare earth upconversion luminescent nanoparticles: small size and tunable emission/excitation spectra, *Acc. Chem. Res.* 47 (4) (2014) 1001–1009, <https://doi.org/10.1021/acs.accounts.4b00144>.

- 1021/ar400218t.
- [30] S. Wu, G. Han, D.J. Milliron, S. Aloni, V. Altoe, D.V. Talapin, et al., Non-blinking and photostable upconverted luminescence from single lanthanide-doped nanocrystals, *Proc. Natl. Acad. Sci. U. S. A.* 106 (27) (2009) 10917–10921, <https://doi.org/10.1073/pnas.0904792106>.
- [31] P. Zhang, W. Steelant, M. Kumar, M. Scholfield, Versatile photosensitizers for photodynamic therapy at infrared excitation, *J. Am. Chem. Soc.* 129 (15) (2007) 4526–4527, <https://doi.org/10.1021/ja0700707>.
- [32] C. Liu, W. Ma, Z. Gao, J. Huang, Y. Hou, C. Xu, et al., Upconversion luminescence nanoparticles-based lateral flow immunochromatographic assay for cephalexin detection, *J. Mater. Chem. C* 2 (45) (2014) 9637–9642, <https://doi.org/10.1039/c4tc02034k>.
- [33] X. Wang, K. Liu, G. Yang, L. Cheng, L. He, Y. Liu, et al., Near-infrared light triggered photodynamic therapy in combination with gene therapy using upconversion nanoparticles for effective cancer cell killing, *Nanoscale* 6 (15) (2014) 9198–9205, <https://doi.org/10.1039/c4nr02495h>.
- [34] L. Huang, G. Han, Near infrared boron dipyrromethene nanoparticles for opto-theranostics, *Small Methods* 2 (9) (2018) 1700370, <https://doi.org/10.1002/smt.201700370>.
- [35] Y. Ma, J. Bao, Y. Zhang, Z. Li, X. Zhou, C. Wan, et al., Mammalian near-infrared image vision through injectable and self-powered retinal nanoantennae, *Cell* 177 (2) (2019) 243–255 e15 <http://www.sciencedirect.com/science/article/pii/S0092867419301011>.
- [36] Y. Zhang, P. Huang, D. Wang, J. Chen, W. Liu, P. Hu, et al., Near-infrared-triggered antibacterial and antifungal photodynamic therapy based on lanthanide-doped upconversion nanoparticles, *Nanoscale* 10 (33) (2018) 15485–15495, <https://doi.org/10.1039/C8NR01967C>.
- [37] H. Guo, H. Qian, N.M. Idris, Y. Zhang, Singlet oxygen-induced apoptosis of cancer cells using upconversion fluorescent nanoparticles as a carrier of photosensitizer, *Nanomedicine* 6 (3) (2010) 486–495, <https://doi.org/10.1016/j.nano.2009.11.004>.
- [38] C. Wang, H. Tao, L. Cheng, Z. Liu, Near-infrared light induced in vivo photodynamic therapy of cancer based on upconversion nanoparticles, *Biomaterials* 32 (26) (2011) 6145–6154, <https://doi.org/10.1016/j.biomaterials.2011.05.007>.
- [39] Y.I. Park, H.M. Kim, J.H. Kim, K.C. Moon, B. Yoo, K.T. Lee, et al., Theranostic probe based on lanthanide-doped nanoparticles for simultaneous in vivo dual-modal imaging and photodynamic therapy, *Adv. Mater.* 24 (42) (2012) 5755–5761, <https://doi.org/10.1002/adma.201202433>.
- [40] J. Kim, H.R. Cho, H. Jeon, D. Kim, C. Song, N. Lee, et al., Continuous O₂-evolving MnFe₂O₄ nanoparticle-anchored mesoporous silica nanoparticles for efficient photodynamic therapy in hypoxic cancer, *J. Am. Chem. Soc.* 139 (32) (2017) 10992–10995, <https://doi.org/10.1021/jacs.7b05559>.
- [41] X. Chen, Z. Zhao, M. Jiang, D. Que, S. Shi, N. Zheng, Preparation and photodynamic therapy application of NaYF₄:Yb, Tm–NaYF₄:Yb, Er multifunctional upconverting nanoparticles, *New J. Chem.* 37 (6) (2013) 1782–1788, <https://doi.org/10.1039/c3nj00065f>.
- [42] Y. Hou, R. Qiao, F. Fang, X. Wang, C. Dong, K. Liu, et al., NaGdF₄ nanoparticle-based molecular probes for magnetic resonance imaging of intraperitoneal tumor xenografts in vivo, *ACS Nano* 7 (1) (2013) 330–338, <https://doi.org/10.1021/nn304837c>.
- [43] Y. Hou, J. Zhou, Z. Gao, X. Sun, C. Liu, D. Shanguan, et al., Protease-activated ratio metric fluorescent probe for pH mapping of malignant tumors, *ACS Nano* 9 (3) (2015) 3199–3205, <https://doi.org/10.1021/acs.nano.5b00276>.
- [44] H.C. Kolb, M.G. Finn, K.B. Sharpless, Click chemistry: diverse chemical function from a few good reactions, *Angew. Chem.-Int. Edit* 40 (11) (2001) 2004–2021, [https://doi.org/10.1002/1521-3773\(20010601\)40:11<2004::AID-ANIE2004>3.0.CO;2-5](https://doi.org/10.1002/1521-3773(20010601)40:11<2004::AID-ANIE2004>3.0.CO;2-5).
- [45] W.G. Lewis, L.G. Green, F. Grynszpan, Z. Radic, P.R. Carlier, P. Taylor, et al., Click chemistry in situ: acetylcholinesterase as a reaction vessel for the selective assembly of a femtomolar inhibitor from an array of building blocks, *Angew. Chem. Int. Ed.* 41 (6) (2002) 1053–1057, [https://doi.org/10.1002/1521-3773\(20020315\)41:6<1053::AID-ANIE1053>3.0.CO;2-4](https://doi.org/10.1002/1521-3773(20020315)41:6<1053::AID-ANIE1053>3.0.CO;2-4).
- [46] I. Kraljić, S.E. Mohsni, A new method for the detection of singlet oxygen in aqueous solutions, *Photochem. Photobiol.* 28 (1978) 577–581, <https://doi.org/10.1111/j.1751-1097.1978.tb06972.x>.
- [47] S. Onoue, Y. Yamauchi, T. Kojima, N. Igarashi, Y. Tsuda, Analytical studies on photochemical behavior of phototoxic substances; effect of detergent additives on singlet oxygen generation, *Pharm. Res.* 25 (4) (2008) 861–868, <https://doi.org/10.1007/s11095-007-9383-4>.
- [48] J. Huang, Y. Hou, T. Ma, P. Zhang, Y. Li, C. Liu, et al., A novel histochemical staining approach for rare-earth-based nanoprobe, *Adv. Therap.* 1 (1) (2018) 1800005, <https://doi.org/10.1002/adtp.201800005>.
- [49] F. Wang, J. Wang, X. Liu, Direct evidence of a surface quenching effect on size-dependent luminescence of upconversion nanoparticles, *Angew. Chem. Int. Ed.* 49 (41) (2010) 7456–7460, <https://doi.org/10.1002/anie.201003959>.
- [50] J.C. Maziere, P. Morliere, R. Santus, New trends in photobiology (Invited review) – the role of the low-density-lipoprotein receptor pathway in the delivery of lipophilic photosensitizers in the photodynamic therapy of tumors, *J. Photochem. Photobiol. B-Biol.* 8 (4) (1991) 351–360, [https://doi.org/10.1016/1011-1344\(91\)80111-T](https://doi.org/10.1016/1011-1344(91)80111-T).